Geo-Bio Interfaces (2026), **3**, e6, 1–13
doi:10.1180/gbi.2026.10008

CAMBRIDGE UNIVERSITY PRESS

Article

Bioavailability of biogenic iron(III) oxyhydroxides for Fe(III)-reducing bacteria

Laura I. Tenelanda-Osorio, Tsz-Ho Chiu, Eva Kernchen, Andreas Kappler and Muammar Mansor
Department of Geosciences, Eberhard Karls Universität Tübingen, Tübingen, Germany

Abstract

Iron-metabolising bacteria play a key role in the biogeochemical Fe cycle, linking it to the bioavailability and transformation of other bioessential elements such as carbon, nitrogen and phosphorus. Fe(III)-reducing bacteria use Fe(III) as an electron acceptor and Fe(II)-oxidising bacteria oxidise Fe(II) to gain energy, forming biogenic iron(III) oxyhydroxides (BIOS). Little is known about the bioavailability of the Fe(III) associated to BIOS ($BIOS_{Fe(III)}$), limiting predictions of its role in the mobility of other bioessential elements. Here we tested the bioavailability of $BIOS_{Fe(III)}$ as a function of: (1) BIOS origin (phototrophic and mixotrophic/autotrophic nitrate-reduction coupled to Fe(II) oxidation), resulting in a gradient of cell-mineral associations from encrustation to loose attachments; (2) two model Fe(III)-reducing microorganisms, *Shewanella oneidensis* MR-1 and *Geobacter sulfurreducens* PCA; (3) the presence or absence of added organic carbon (lactate or acetate); and (4) before and after freeze-thawing, simulating conditions relevant to temperate environments. Statistical redundancy analysis showed that despite variations in the properties of the BIOS (e.g. particle size, surface areas, organic content) due to its origin and freeze-thaw treatment, organic carbon availability was the main factor controlling $BIOS_{Fe(III)}$ reduction rates and extents. With added organic carbon, $BIOS_{Fe(III)}$ were reduced completely, with faster rates observed for *G. sulfurreducens*, suggesting limited availability of BIOS-associated organic carbon ($BIOS_{OC}$) to these microorganisms. $BIOS_{Fe(III)}$ was also more bioavailable than synthetic 2-line ferrihydrite, attributed to increased redox reactivity originating from $BIOS_{OC}$ (e.g. residual cells and extracellular polymeric substances). Freeze-thawing, a process relevant in high-latitude zones, mountain glaciers and other temperate climate regions across Earth, mostly decreased the rate and extent of $BIOS_{Fe(III)}$ reduction, although the magnitude and direction of the effect depend on the specific variable combination. Thus, we conclude that environmental organic carbon availability is the primary factor controlling the bioavailability of $BIOS_{Fe(III)}$, with subsequent effects on the transformation of other bioessential elements.

Keywords: biogenic iron oxides (BIOS); cryosphere; Fe biogeochemistry; Fe(II)-oxidising bacteria; Fe(III)-reducing bacteria

(Received 25 February 2026 UTC; revised 19 May 2026 UTC; manuscript accepted: 31 May 2026 UTC)

Introduction

Biogenic iron(III) oxyhydroxides (BIOS) are mixtures of Fe(III) nanominerals, cells and extracellular polymeric substances (EPS) produced by Fe(II)-oxidising bacteria (FeOB). The mineral component typically consists of ferrihydrite ($(Fe_{III})_{4\text{-}5}(OH,O)_{12}$, Fh), goethite ($Fe_{III}O(OH)$) and amorphous Fe(III) phosphates depending on the geochemical conditions of the environment or the experimental conditions (Abramov *et al.*, 2022; Angelova *et al.*, 2015; Ferris, 2005; Gault *et al.*, 2012; Kikuchi *et al.*, 2014; Miot *et al.*, 2015, 2009a, 2009b; Nedkov *et al.*, 2016). The organic part is mostly lipid and polysaccharide moieties associated with aliphatic groups in the outer part of the minerals, while carboxylic and aromatic moieties are incorporated within the structure (Chan *et al.*, 2009; Sowers *et al.*, 2019; Whitaker *et al.*, 2021). At circumneutral pH and microoxic conditions, biotic Fe(II) oxidation occurs at a higher rate than abiotic oxidation (Baker *et al.*, 2023). Furthermore, there are numerous observations of orange-coloured microbial mats rich in Fe(III) nanominerals across different environments (Brooks and Field, 2020; Garber *et al.*, 2021). Hence, BIOS represent a significant component of Fe(III) oxyhydroxide minerals in environments where FeOB are present.

The concept of a 'rusty carbon sink' has been explored extensively in recent years, underscoring the importance of Fe(III) (oxyhydr) oxides in controlling the bioavailability of organic carbon (OC) (Goebel *et al.*, 2005; Yudina and Kuzyakov, 2019). On average, about 40% and 19% of the total organic carbon (TOC) is associated with Fe in terrestrial soils and marine sediments, respectively (Jia *et al.*, 2024; Lalonde *et al.*, 2012). These Fe(III) minerals can be altered by Fe(III)-reducing bacteria (FeRB) that reduce Fe(III) to Fe(II) coupled to the oxidation of electron donors such as OC, CH_4, H_2 or sulfur species (Chen *et al.*, 2025; Kappler *et al.*, 2021; Knoll, 2012; Konhauser *et al.*, 2011). The extent of Fe(III) reduction is governed by the crystallinity and size of the minerals, and the availability of biodegradable OC (Roden, 2003, 2004; Xu *et al.*, 2025). Intriguingly, the Fe(III) associated with BIOS ($BIOS_{Fe(III)}$) has been shown to be more bioavailable

Corresponding author: Muammar Mansor; Email: muammar.mansor@uni-tuebingen.de
Cite this article: Tenelanda-Osorio L.I., Chiu T.-H., Kernchen E., Kappler A., & Mansor M. (2026). Bioavailability of biogenic iron(III) oxyhydroxides for Fe(III)-reducing bacteria. *Geo-Bio Interfaces* **3**, e6, 1–13. https://doi.org/10.1180/gbi.2026.10008

© The Author(s), 2026. Published by Cambridge University Press on behalf of The Mineralogical Society of the United Kingdom and Ireland. This is an Open Access article, distributed under the terms of the Creative Commons Attribution licence (http://creativecommons.org/licenses/by/4.0), which permits unrestricted re-use, distribution and reproduction, provided the original article is properly cited.

for microbial reduction than that in synthetic Fe(III) (oxyhydr) oxides (Ferris, 2005; Langley *et al.*, 2009a, 2009b; Straub *et al.*, 1998). The increased reactivity is attributed to the lower crystallinity and higher surface area of BIOS compared to synthetic Fe(III) (oxyhydr)oxides (Chan *et al.*, 2009; Miot *et al.*, 2015; Toner *et al.*, 2009; Whitaker et al., 2021). Specifically, Langley *et al.* (2009a) found that *Shewanella putrefaciens* CN32 reduced BIOS twice as quickly as synthetic 2-line ferrihydrite. Moreover, BIOS of different origins exhibit different reactivity – $BIOS_{Fe(III)}$ from *Leptothrix* spp. were reduced twice as fast as those from field sites dominated by *Gallionella* spp. (Langley *et al.*, 2009a; Najem *et al.*, 2016). These studies raised the question as to whether other BIOS will also display different bioavailability depending on their origin, and why (*i.e.* due to variable crystallinity and organic association). Furthermore, as diverse FeRB species exist in nature, there is the question of whether different BIOS might exhibit varying reactivity to different FeRB.

The 'rusty carbon sink' concept is especially relevant to environments undergoing rapid thawing, such as in high-latitude zones and mountain glaciers. As ice thaws due to climate change, previously buried OC is suddenly at risk of being decomposed into greenhouse gases such as CO_2 and CH_4. Association of OC with Fe(III) (oxyhydr)oxides typically results in protection of the OC from microbial degradation (Adhikari *et al.*, 2019). The decomposition rate of glucose, for instance, is >99.5% faster for free glucose in soil than in glucose adsorbed on synthetic ferrihydrite (Porras *et al.*, 2018). Nonetheless, the reductive dissolution of Fe(III) (oxyhydr) oxides by FeRB releases Fe-associated OC that can be further metabolised to simple OC (*e.g.* acetate, lactate), CO_2 and CH_4 (Adhikari *et al.*, 2017; Tian *et al.*, 2025). This association is also observed in biofilms, where FeRB typically reside close to or within biofilms of FeOB, together contributing to a biological Fe cycle on small spatial scales (Brooks and Field, 2020; Garber *et al.*, 2021). At the moment, there is limited knowledge on whether BIOS-associated OC ($BIOS_{OC}$) can be degraded or released by FeRB.

In high latitudes and mountain glaciers, as well as in temperate climate regions across Earth, soils undergo regular freeze-thaw cycles that affect Fe–OC associations (Patzner *et al.*, 2020 and 2022). On the one hand, freeze-thawing is known to facilitate aggregation (Wu *et al.*, 2022) and to slow down mineral transformation due to the lower temperature (Mullin, 2004; Putnis, 2009). On the other hand, freeze-thawing can also accelerate mineral transformation by generating high surface area fractures or promoting localised high ion concentrations (*e.g.* O_2, H^+, Fe^{2+}) in microenvironments around the minerals (Jeong *et al.*, 2015; Sebaaly *et al.*, 2025; Zhai *et al.*, 2021). Freeze-thawing can also promote the release of OC from mineral aggregates (Wu *et al.*, 2022) or promote the degradation of complex OC (Fellman *et al.*, 2008; Pokrovsky *et al.*, 2018; Payandi-Rolland *et al.*, 2021), potentially increasing its bioavailability. Hence, freezing causes a variety of interrelated effects in soils, necessitating laboratory experiments to quantify its net effects on the bioavailability of Fe(III). BIOS are also exposed to freeze-thawing. Thus, controlled laboratory experiments using freeze-thawed BIOS are necessary to directly quantify the net Fe(III) reduction rate and extent, as well as providing mechanistic insights into how changes in properties relate to changes in bioavailability.

In this study, we investigated the bioavailability of BIOS as a function of multiple variables: three origins of BIOS, two FeRB, with and without added OC, and before and after freeze-thawing. This combination of variables resulted in a total of 24 setups, allowing us to investigate the bioavailability of BIOS with wide implications across diverse environmental systems. Under some conditions, we also compared the bioavailability of BIOS to synthetic ferrihydrite, underlining the importance of performing experiments with naturally relevant materials to avoid interpretation based solely on pure lab-synthesised minerals.

Methods

Fe(III) mineral sources

All glassware used for cultures was washed in acid (1 M HCl), then rinsed three times with double deionised water (DDI, Millipore, >18 MΩ cm^{-1}), and subsequently baked at 180°C for 4 h and 30 min prior to use. Sampling was conducted under aseptic and anoxic conditions in a glovebox (MBraun Unilab Workstation, 100% N_2 atmosphere).

BIOS were obtained from three Fe(II)-oxidising bacteria strains with different Fe(II) oxidation mechanisms: photoferrotrophy by *Rhodopseudomonas palustris* TIE-1 (hereafter TIE-1), chemoautotrophy coupled to nitrate reduction by enrichment culture KS (hereafter KS) and mixotrophy coupled to nitrate reduction by *Acidovorax* sp. BoFeN1 (hereafter BoFeN1) (Fig. 1; Text S1). The FeOB were grown in 22 mM bicarbonate-buffered mineral medium at pH 7 (Ehrenreich and Widdel, 1994) in 100 mL serum bottles with 50 mL headspace of N_2/CO_2 (90:10 v/v) in the dark at 28°C for BoFeN1 and KS, and at 20°C under illumination for TIE-1. The BoFeN1 medium had a lower phosphate concentration (1 mM) in addition to 3.5 mM NaCl to maintain the ionic strength in the medium. It was then amended with 10 mM Fe(II) (as Fe_2Cl), 6 mM NO_3^- (as $NaNO_3$) and 2 mM acetate (as CH_3COONa). KS medium was amended with 10 mM Fe(II) and 2 mM NO_3^-. TIE-1 medium was amended with 3 mM Fe(II), *i.e.* a lower initial Fe(II) concentration than the other strains, because of its faster metabolism at this concentration. We acknowledge that at lower Fe(II) concentrations TIE-1 BIOS are richer in ferrihydrite, while at higher concentrations and therefore longer incubation time, TIE-1 BIOS have a higher proportion of crystalline minerals due to recrystallisation and reaction with the Fe(II) in solution (Jiao *et al.*, 2005; Nikeleit *et al.*, 2024). The media were inoculated with 1% (v/v) of a preculture in the case of KS, 5% (v/v) of BoFeN1 and 3% (v/v) of TIE-1. Precultures were grown in the same conditions as described above.

For native BIOS experiments, BIOS were collected when the Fe(II)/Fe(total) ratio was 5.7 ± 1.5%, 8.0 ± 2.0% and 7.0 ± 0.2% for TIE-1, BoFeN1 and KS, respectively, indicating near complete oxidation. For experiments with freeze-thawed BIOS, the initial Fe(II)/Fe(total) ratio for BIOS of TIE-1, BoFeN1 and KS was 6.9 ± 0.6%, 13.4 ± 0.3% and 27.1 ± 0.5%, respectively. This corresponded to 6 days of incubation for BoFeN1 and KS, and 12 days for TIE-1. To collect the BIOS, the serum bottles with the cultures were centrifuged at 12,045 *g* for 2 min and the supernatant was exchanged with fresh FeRB medium (composition detailed below). This was repeated three times for each bottle. After the last centrifugation, the supernatant was removed and all the BIOS were finally collected, resuspended with FeRB medium, and stored anoxically and aseptically at 4°C. For freeze-thawed BIOS setups, the 200 mL serum bottles containing BIOS (after washing) were left in a freezer at –20°C for 13 days. After this time, the bottles were left to thaw at room temperature before transferring the BIOS for the Fe(III) reduction experiments with FeRB, keeping the anoxic and aseptic conditions.

Two-line ferrihydrite was synthesised according to Schwertmann and Cornell (2008). First, 40 g of $Fe(NO_3)_3$ $9H_2O$ was dissolved in 500 mL of MilliQ water and the pH of the solution

https://doi.org/10.1180/gbi.2026.10008 Published online by Cambridge University Press

was adjusted to 7.3 by titration with 1 M KOH. After 2 h of incubation, the pH of the solution was adjusted to 7.5 with KOH. The minerals were washed four times with MilliQ water before resuspension in water to a concentration of ~335 mM Fe total.

Cultivation of FeRB and experimental setup

Fe(III)-reducing bacteria have developed multiple mechanisms to reduce Fe(III), including direct contact between minerals and the cell membrane, conductive pili, electron shuttles and chelation. Here we tested BIOS bioavailability for FeRB *Shewanella oneidensis* MR-1 (hereafter *S. oneidensis*) and *Geobacter sulfurreducens* PCA (hereafter *G. sulfurreducens*) as model organisms whose primary reduction mechanisms differ (electron shuttles and direct cell-mineral contact, respectively; Text S2). The FeRB were grown in 30 mM bicarbonate-buffered mineral medium at pH 7 (Ehrenreich and Widdel, 1994) in 100 mL serum bottles with 50 mL headspace of N_2/CO_2 (90:10 v/v %) in the dark at 28°C. Six bottles were amended with ~6 mM of $BIOS_{Fe(III)}$ from each of the three FeOB (18 bottles in total). Of these, nine bottles were amended with ~4 mM of an additional carbon source: acetate for *G. sulfurreducens* and lactate for *S. oneidensis*. The same setup applies for experiments with freeze-thawed BIOS. The initial cell concentration in the experiment was ~5×10^5 cells mL^{-1}, achieved by inoculating the media with 5% (v/v) of a preculture containing ~10^7 cells mL^{-1} of each FeRB strain. Cell concentration was calculated using optical density (OD) and calibration curves from our laboratory in the case of *S. oneidensis* (OD = 0.095 ± 0.002) and from Kubannek *et al.* (2020) in the case of *G. sulfurreducens* (OD = 0.17 ± 0.04). Precultures were grown using fumarate as an electron acceptor. Duplicates of FeRB cultures with ~5 mM acetate/lactate as an electron donor and ~6 mM ferrihydrite as an electron acceptor were set up to check for cell viability in some cases. Negative controls for both setups (with and without carbon) contained ~6 mM of Fe(III) of each BIOS and acetate/lactate as stated above.

Geochemistry

Every 2 days, 4 mL of sample were taken from each replicate during the first 12 days with a syringe under anoxic conditions in a glovebox. Because of the lower Fe(III) reduction rate of *S. oneidensis*, sampling was done every 4–7 days after day 12. Samples were split into two vials, one for centrifugation at 12,045 *g* for 5 min and the other one (without centrifugation) for Fe(II) and Fe(total) content (150 µL). From the supernatant of the centrifuged samples, aliquots were taken for dissolved OC (in the form of non-purgeable OC) and Fe^{2+} content. Samples for Fe measurements were diluted 1:1 with 1 M HCl inside the glovebox and further diluted with 1 M HCl prior to analysis.

Fe content (Fe^{2+}, Fe(II) and Fe total) was quantified in triplicate by colorimetry using the ferrozine assay (Hegler *et al.*, 2008; Stookey, 1970). For quantification of Fe(II) and Fe^{2+}, 20 µL of sample were added to 80 µL of 1 M HCl in a 96-well plate followed by 100 µL of ferrozine reagent. After 5 min, the ferrozine–Fe(II) complex was measured at 562 nm in a plate reader (Multiskan GO; Thermo Fisher Scientific). For Fe total (Fe(tot)), 20 µL of sample were added to 80 µL of hydroxylamine hydrochloride (10% w/v in 1 M HCl) in a 96-well plate. After 30 min of reaction, the ferrozine reagent was added, and the ferrozine-Fe(II) complex was measured after 5 min of incubation. All samples were measured in triplicate and in the dark. Each 96-well plate also contained triplicates of 50, 100, 200, 400, 600, 800 and 1000 µM Fe(II) ethylenediammonium sulfate tetrahydrate for standard curve calibration. The aliquot for dissolved OC concentration was diluted 1:4 in 80 mM HCl and measured in triplicate with a TOC analyser (multi N/C 2100S; Analytik Jena AG). Each run contained standards of 5, 10, 20 and 40 mg L^{-1} OC for calibration.

Solid phase analysis

Four aliquots of 2–5 mL each from the washed BIOS and from the freeze-thawed BIOS were centrifuged, and the supernatant was discarded. The solids were then dried (>24 h) and stored under anoxic conditions until total carbon analysis, surface area analysis, µ-X-ray diffraction (µ-XRD) and Mössbauer spectroscopy.

The TOC content in the solid phase was determined in duplicate with a soliTOC (Cube; Elementar). The specific surface area (SSA) was determined with the Brunauer–Emmett–Teller equation (Brunauer *et al.*, 1938) by adsorption/desorption of N_2 using a Micromeritics Gemini VII surface area and porosity analyser (Micromeritics Instrument Corporation). At partial pressures ranging from 0.05 to 0.3 P/P_0 and at 77 and 298 K, N_2 adsorption was quantified from outgassed samples over a 24 h period.

µ-XRD was performed with a Bruker D8 Discover GADDS XRD2 micro-diffractometer equipped with a standard sealed tube with a Co-anode (CoKα radiation, λ = 0.17903 nm, 30 kV/30 mA). The measurement time was 240 s at detector positions 15° and 40°. Resulting diffractograms were analysed using the software Match! (version 3.6.2.121). Crystallite size (D) was calculated using the Scherrer equation (Patterson, 1939):

$$D = \frac{k\lambda}{B}\cos(\theta) \quad (1)$$

where k is the Scherrer constant (assumed to be 0.9), λ is the X-ray wavelength (0.1789 nm for CoKa) and B is the full-width half-maximum (FWHM) of the diffraction peak.

The identification of Fe phases within the BIOS was performed by Mössbauer spectroscopy. The dried BIOS were homogenised by mortar and pestle in the glovebox before loading them into Plexiglas holders (area 1 cm^2), forming a thin disc. The holders were frozen and stored anoxically until analysis. Holders were inserted into a closed-cycle exchange gas cryostat (Janis cryogenics) under a backflow of He gas to minimise exposure to air. Spectra were collected at 77 and 30 K using a constant acceleration drive system (WissEL) in transmission mode with a ^{57}Co/Rh source. All spectra were calibrated against a 7 µm thick α-^{57}Fe foil that was measured at room temperature. Analysis was carried out using Recoil (University of Ottawa) and the extended Voigt based fitting routine (Lagarec and Rancourt, 1997). The half width at half maximum was constrained to 0.122 mm s^{-1} during the fitting process.

Size-distribution analysis

Particle size was measured for the original and freeze-thawed BIOS. The unfiltered particulate fraction was measured using a particle size analyser (Mastersizer 2000; Malvern Instruments) with distilled water as dispersant, adding the samples directly from the serum bottles with the cultures, 1 mL at a time with a pipette until the obscuration was between 10% and 20% in the Hydro 2000S dispersion unit (total volume of 150 mL). A total of 10, 18 and 4 mL were added for the original BIOS of BoFeN1, TIE-1 and KS, respectively. For the freeze-thawed BIOS, 12, 15 and 8 mL were

https://doi.org/10.1180/gbi.2026.10008 Published online by Cambridge University Press

added for BoFeN1, TIE-1 and KS, respectively. Measurements were conducted four times per sample, on duplicate samples, with three cleaning cycles in between each sample.

The particle size and zeta potential of the colloidal fraction (operationally defined as <1.2 µm based on the filter size) was measured by dynamic light scattering using a Zetasizer Nano (Malvern Instruments) with three runs of 20 s each. Samples were collected in a glovebox by passing an aliquot of 2 mL through a 1.2 µm pore size filter (Acrodisc 32 mm syringe filter) and stored there until measurement. Then, 0.9 mL of the filtered samples were placed in a DTS1070 disposable folded capillary cell for both size (three runs, 20 s each) and surface charge (three runs, 50 scans each) analysis. The attenuation and voltage parameters were determined automatically by the instrument. The measured electrophoretic mobility was converted to surface charge using the Smoluchowski method (Hunter, 1981).

Scanning electron microscopy

At the end of the incubation of FeOB, BIOS were collected and imaged with a Scanning Electron Microscope (SEM). An aliquot of 200 µL of sample were fixed in 2.5 %(aq) electron microscopy-grade glutaraldehyde and sequentially dehydrated with 25%, 50% 75%, and 100% (v/v) ethanol and finally 100% (v/v) hexamethyldisilazane (HMDS) on a round glass coverslip previously coated with a 0.01% w/v solution of Poly-L-Lysine to provide a hydrophilic surface for attachment. The samples on the glass slide were dried overnight and attached to aluminium stubs using carbon adhesive tabs. This was then sputter-coated with a 10 nm gold layer (sputtering 50 s at 5×10^{-2} mbar, 30 mA, and a working distance of 35 mm) using a BAL-TEC SCD 005 sputter coater. Imaging was performed with a ZEISS Crossbeam 550/5502 L, with an acceleration voltage of 5 kV, and the SESI (secondary electrons–secondary ions) detector.

Statistical analysis

Analysis of variance to test significant differences between treatments was performed in Origin 2025 (OriginLab Co.). The Fe(III) reduction extents reported here and used for calculations refer to the Fe(II)/Fe(total) ratios that were not subtracted with the ratios at time point 0. The Fe(III) reduction rates were calculated from the linear phase of the reduction rate, excluding the lag phase (which could cause potential biases from initial inoculation) and the stationary phase when Fe(III) reduction had stopped. The redundancy analysis (RDA) was performed in CANOCO 5 software (Microcomputer Power Co.).

Results

BIOS characterisation before and after freeze-thawing

Mineralogy and cell-mineral associations

In this study, we subjected original and freeze-thawed BIOS from three different FeOB with different metabolisms to reduction by FeRB. BIOS were first characterised through a suite of analytical techniques before the reduction experiments. All BIOS consisted of a mixture of different Fe(III) oxyhydroxides with varying crystallinities. Micro-XRD indicated that goethite was the primary crystalline phase in all FeOB (Fig. S1). Vivianite was also present in KS, but its origin is abiotic because of the precipitation of Fe(II) and phosphate initially present in the medium (4 mM). Mössbauer spectroscopy showed that KS BIOS had the most complex composition with more than 50% of the minerals as ferrihydrite. In BoFeN1 and TIE-1 BIOS, poorly crystalline minerals such as ferrihydrite and lepidocrocite were together present in higher proportions than that of crystalline goethite (Figs S2, S3; Text S3; Table S1). SEM images showed an increasing degree of cell encrustation with minerals in the order of TIE-1 < KS < BoFeN1 (Fig. 1). The mineralogical assemblages and cell-mineral associations are

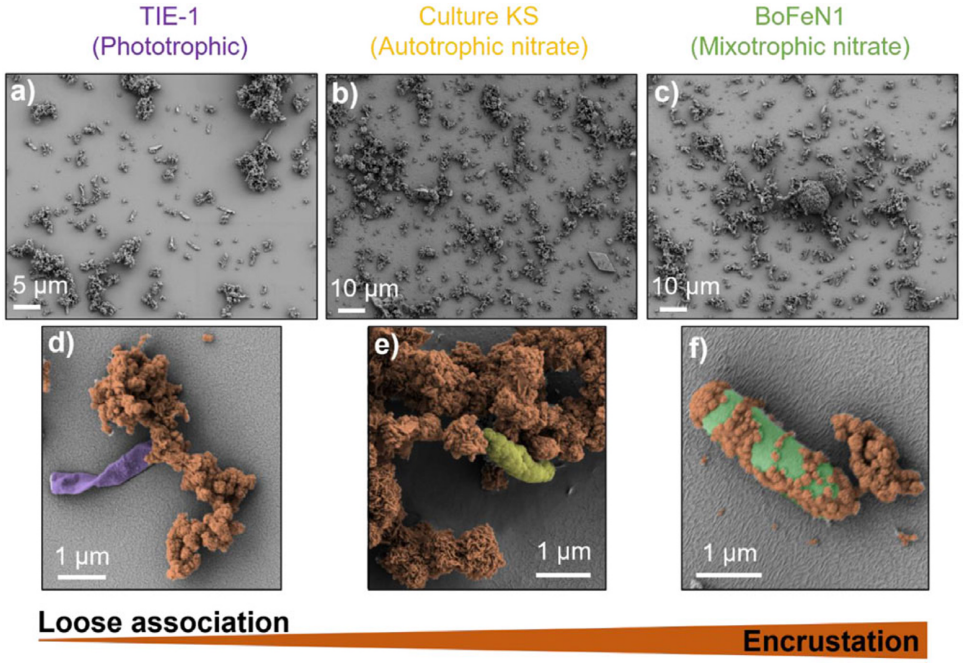


Figure 1. Scanning electron micrographs of biogenic iron oxides used in this study. Overview of (a) *Rhodopseudomonas palustris* TIE-1 (TIE-1), (b) enrichment culture KS (KS) and (c) *Acidovorax* sp. BoFeN1 (BoFeN1). Close-up false colour images show that (d) TIE-1 (purple) has loose cell-mineral associations. (e) KS (yellow) has partial associations with some cells of the flanking community being encrusted. In the image, one representative fully encrusted cell, with characteristic granular surface made by the precipitated Fe(III) (oxyhydr)oxides is shown. (f) BoFeN1 (green) has high degree of encrustation.

https://doi.org/10.1180/gbi.2026.10008 Published online by Cambridge University Press

broadly consistent with what has been observed in past studies (Texts S1 and S4). Freeze-thawing led to no changes in mineralogy (Table 1) and goethite remained the primary crystal phase in the system, in addition to vivianite in the case of KS (Fig. S1).

Particle-size distribution, specific surface area and zeta potential

The SSA of the BIOS ranged from 75.1 to 144.4 $m^2\ g^{-1}$, with the highest value observed for TIE-1 (Table 2). The particulate size distribution of unfiltered BIOS in this study ranged from hundreds of nanometres to a few hundred micrometres (up to ~2000 μm for TIE-1). In the case of TIE-1, we observed two size fractions, one with a mean diameter of 23 μm and another one with a mean diameter of 1553 μm (Table 2). These are larger than the values for BoFeN1 (12.8 ± 1.4 μm) and KS (7.9 ± 0.3 μm).

We also analysed colloidal Fe(III) oxyhydroxides (fractions <1.2 μm in size), as these are typically the most reactive fractions. Ferrozine analysis showed that this fraction constituted <5% of the total Fe. The colloidal mean sizes were 1088 ± 186, 675 ± 130 and 550 ± 28 nm for TIE-1, KS and BoFeN1, respectively. Their zeta potentials were mostly negative (–1 to –5.3 mV, with one outlier at 5.4 mV), consistent with the presence of organics on the surface of the Fe(III) minerals (Table 2).

Freeze-thawing led to changes in the physiochemical parameters, resulting in consistently more negative zeta potential (–17 to –7 mV across all three FeOB). The effects on particle size and SSA were FeOB-specific. For SSA, that of BoFeN1 increased to 180.5 $m^2\ g^{-1}$, while it decreased to 98.4 and 55.2 $m^2\ g^{-1}$ in TIE-1 and KS, respectively. For particulate size distribution of unfiltered samples, the mean size of the smaller size group of TIE-1 BIOS remained unchanged, but the larger aggregates (1553 μm) decreased to an average size of 209 μm. Meanwhile, the mean size of both BoFeN1 and KS particulates increased to 17.4 ± 0.0 and 138 μm, respectively (Fig. S4). Finally, the colloidal size distribution decreased after freeze-thawing for TIE-1 (290 ± 7 nm) and KS (833 ± 101 nm), while it increased for BoFeN1 (491 ± 48 nm).

Carbon content in the solid phase

The TOC in the solid-phase fraction of BIOS – corresponding to EPS and cells remaining after washing – is reported in Table 2. TIE-1 has the highest TOC (2.2%), followed by BoFeN1 (1.3%) and KS (0.24%). In our study, we found that freeze-thawing decreased significantly ($n = 3$ for original, $n = 2$ for freeze-thawed, $\alpha = 0.05$) the TOC in the BIOS of TIE-1 to 1.5% and KS to 0.16%, while TOC in the BIOS of BoFeN1 remained unchanged (1.3%). Because of the low concentration of TOC across all setups, the characteristic bacterial Fourier transform infrared spectrum was overwhelmed by bands that can be attributed to Fe(III) minerals (data not shown).

Table 1. Crystallite size (nm) of BIOS as determined from the Scherrer equation (Eq. 1) based on μ-XRD reflection patterns.

			TIE-1		BoFeN1		KS	
Mineral phase	°2θ	Replicate	Original	Freeze-thawed	Original	Freeze-thawed	Original	Freeze-thawed
Goethite	25	a	9.58	13.32	10.73	10.88	–	–
		b	–		9.67			
Goethite	63	a	11.39	9.30	15.51	19.05	29.34	12.34
		b	8.90		14.86		17.02	
Vivianite	15	a					12.98	16.16
		b					14.96	

Grey values indicate lower values when comparing original vs freeze-thawed BIOS. BIOS = Biogenic iron(III) oxyhydroxides; BoFeN1 = *Acidovorax* sp. BoFeN1; KS = enrichment culture KS; TIE-1 = *Rhodopseudomonas palustris* TIE-1; XRD = X-ray diffraction.

Table 2. Mean particulate size, specific surface area (SSA), total organic carbon (TOC), zeta potential and mean colloidal size (nm) of biogenic iron oxides (BIOS), original and after freeze-thawing, with additional values from the literature for *Thiodictyon* sp. strain F4 (F4), *R. ferrooxidans* sp. strain SW2 (SW2) and *Gallionella*-like environmental BIOS from groundwater (GL).

	TIE-1		BoFeN1		KS		F4	SW2	GL
	Original	Freeze-thawed	Original	Freeze-thawed	Original	Freeze-thawed			
Mean particulate size (μm)	23; 1553	23.8 ± 0.8; 209[d]	12.8 ± 1.4[d]	17.4 ± 0.0[d]	7.9 ± 0.3[d]	138	10–40[a]	10–40[a]	
SSA (m^2/g)	144.4	98.4	80.4	180.5	75.1	55.2		286[f]	
			158[a]						
TOC (wt%)	2.2 ± 0.2	1.5 ± 0.03	1.3 ± 0.0	1.3 ± 0.0	0.24 ± 0.01	0.16 ± 0.001		[C] = ([Fe]–100)/2.5[b]	1.2[c]
Zeta potential (mV)	–3.35 ± 0.35[d]	–8.00 ± 1.0[e]	–3.15 ± 0.25[d]	–8.45 ± 0.55[e]	5.40 ± 1.20	–16.10 ± 1.10[e]			
					–4.60 ± 2.30				
Mean colloidal size (nm)	1087.5 ± 186[d]	290 ± 7[d]	550 ± 28[d]	491 ± 48[d]	675 ± 130[d]	833 ± 101[e]			

Grey values indicate the smaller absolute value when comparing original and freeze-thawed BIOS. BoFeN1 = *Acidovorax* sp. BoFeN1; KS = enrichment culture KS; TIE-1 = *Rhodopseudomonas palustris* TIE-1.
[a]Kappler *et al.* (2005).
[b]Relationship of Fe–carbon (C) concentration in the extracellular filaments of the photoferrotroph *Rhodobacter* sp. strain SW2 as reported by Miot *et al.* (2009a).
[c]Cismasu *et al.* (2016).
[d]Replicate bottles = 2.
[e]Replicate bottles = 3.
[f]Piepenbrock *et al.* (2014).

https://doi.org/10.1180/gbi.2026.10008 Published online by Cambridge University Press

BIOS as electron donor and acceptor

We incubated the FeRB, *S. oneidensis* and *G. sulfurreducens* without the addition of bioavailable OC sources to test the bioavailability of BIOS as both electron donor and acceptor. In the negative controls, the Fe(II)/Fe(total) ratio remained at 6.9 ± 2.3%, 15.4 ± 4.9% and 9.9 ± 4.5% with original BIOS of TIE-1, BoFeN1 and KS, respectively. At the end of the reduction experiment, the Fe(II)/Fe(total) ratio reached a maximum of 52% (Fig. 2). BoFeN1 BIOS were the most bioavailable, with a higher Fe(III) reduction extent with both FeRB, followed by TIE-1 and finally KS. BIOS of BoFeN1, TIE-1 and KS were reduced to 52%, 44% and 36% by *G. sulfurreducens*, respectively; and up to 43%, 34% and 31% for BIOS of BoFeN1, TIE-1 and KS by *S. oneidensis*, respectively (Table S2). In the setup with *G. sulfurreducens*, the maximum extent was reached within 10 days, at a rate of 0.16, 0.41 and 0.23 mM Fe (II) day^{-1} for BIOS of TIE-1, BoFeN1 and KS, respectively (Fig. 2a; Table S2). *S. oneidensis* reduced $BIOS_{Fe(III)}$ in 40 days, with a lower rate of 0.09, 0.05 and 0.08 mM Fe(II) day^{-1} for BIOS of TIE-1, BoFeN1 and KS, respectively (Fig. 2b; Table S2). Note, however, that despite the absence of additional OC in the setups, the preculture carried leftover OC (*e.g.* acetate, lactate) that probably served as an electron donor (see Discussion, section *Bioavailable OC controls the extent of BIOS Fe(III) reduction*).

Fe(III) reduction in the presence of available electron donors

To investigate if OC was the factor limiting $BIOS_{Fe(III)}$ reduction, 5 mM lactate or acetate were introduced into the setups as electron donors for S. *oneidensis* and G. *sulfurreducens*, respectively. In the negative control with lactate, the Fe(II)/Fe(total) ratios of original BIOS of TIE-1, BoFeN1 and KS remained at 6.3 ± 1.8%, 15.6 ± 4.9% and 7.3 ± 1.9%, respectively. In the negative control with acetate, the Fe(II)/Fe(total) ratios of BIOS of TIE-1, BoFeN1 and KS remained at 6.8 ± 1.1%, 18.3 ± 4.0% and 8.0 ± 2.9%, respectively. Both strains were able to reduce 100% of the $BIOS_{Fe(III)}$ in all cases. *G. sulfurreducens* reduced the BIOS significantly (n = 3, α = 0.05) faster than *S. oneidensis*, reducing them within 10 days with rates of 0.72, 0.69 and 0.44 mM Fe (III) day^{-1} for TIE-1, BoFeN1 and KS BIOS, respectively (Fig. 3a; Table S3). *S. oneidensis* took longer to reduce the $BIOS_{Fe(III)}$ (within 40 days) with rates of 0.13, 0.12 and 0.15 mM Fe(III) day^{-1} for TIE-1, BoFeN1 and KS BIOS, respectively (Fig. 3b; Table S3). In these setups, we also performed additional incubations with synthetic ferrihydrite as the Fe(III) source. For both FeRB, we observed a much slower reduction rate of ferrihydrite relative to the BIOS, and similar between the FeRB, 0.07 ± 0.01 and 0.08 ± 0.00 mM Fe(III) day^{-1} with *G. sulfurreducens* and *S. oneidensis*, respectively (Fig. 3; Table S3).

Effect of freeze-thawing on Fe(III) reduction

We tested the impact of freeze-thawing on the bioavailability of BIOS. The results showed that the Fe(II)/Fe(total) ratio in negative controls remained 9.4 ± 4.0%, 15.6 ± 9.1% and 28.3 ± 8.6% with freeze-thawed BIOS of TIE-1, BoFeN1 and KS, respectively, without any additional electron donor. *G. sulfurreducens* reached maximum $BIOS_{Fe(III)}$ reduction extents of 49%, 40% and 40% for BIOS

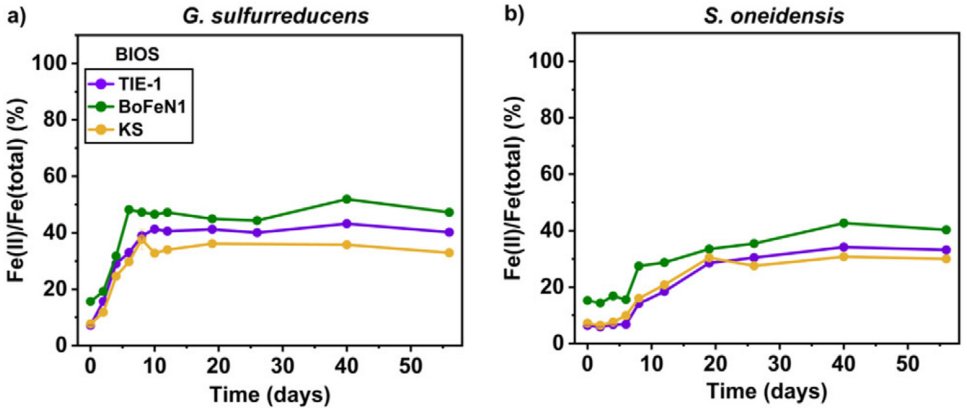


Figure 2. Fe(II)/Fe(total) ratio of the reduction of ~6 mM $BIOS_{Fe(III)}$ by (a) *G. sulfurreducens* and (b) *S. oneidensis* without additional acetate or lactate. Data shown are the mean of experimental triplicates; error bars that indicate the standard deviations (n = 3) are smaller than the symbols in the figures.

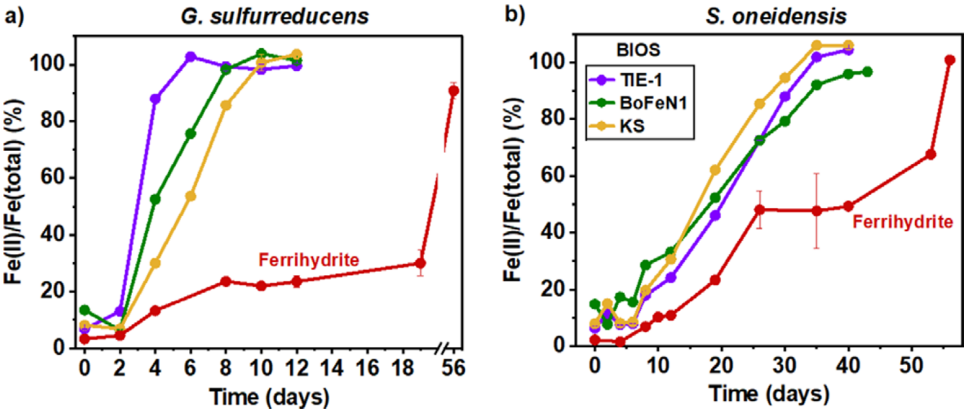


Figure 3. Fe(II)/Fe(total) ratio of the reduction of ~6 mM $BIOS_{Fe(III)}$ (mixture of ferrihydrite, goethite and lepidocrocite) and synthetic two-line ferrihydrite by (a) *G. sulfurreducens* and (b) *S. oneidensis* in the presence of 5 mM of acetate or lactate, respectively. Shown are the means of experimental triplicates for BIOS and duplicates for ferrihydrite; error bars (in most cases smaller than and hidden by the symbols) indicate the standard deviation (n = 3).

https://doi.org/10.1180/gbi.2026.10008 Published online by Cambridge University Press

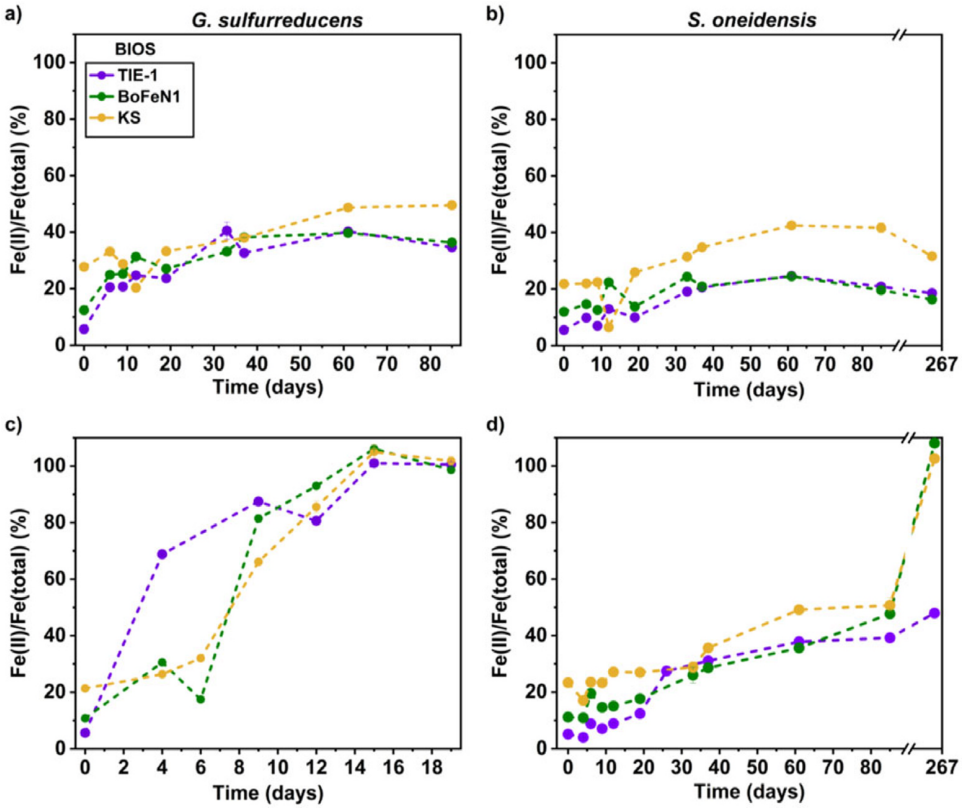


Figure 4. Fe(II)/Fe(total) ratio of freeze-thawed $BIOS_{Fe(III)}$ reduction by (a) *G. sulfurreducens* and (b) *S. oneidensis* without additional carbon and in the presence of 5 mM of acetate and lactate for (c) *G. sulfurreducens* and (d) *S. oneidensis*, respectively. Data shown are the mean of experimental triplicates for BIOS and error bars (in most cases hidden by the symbols) indicate the standard deviation.

of KS, BoFeN1 and TIE-1, respectively (Table S2), within 61 days (Fig. 4a). Within the same period, *S. oneidensis* reached maximum $BIOS_{Fe(III)}$ reduction extents of 43%, 25% and 25% for BIOS of KS, BoFeN1 and TIE-1, respectively (Fig. 4b). In all setups, the Fe(III) reduction rates between the two FeRB were statistically different ($n = 3$, $\alpha = 0.05$). *G. sulfurreducens* was faster at reducing $BIOS_{Fe(III)}$ from TIE-1, BoFeN1 and KS at 0.09 ± 0.02, 0.06 ± 0.01 and 0.29 ± 0.06 mM Fe(III) day^{-1}, respectively, while *S. oneidensis* reduced them at 0.03 ± 0.01, 0.04 ± 0.02 and 0.24 ± 0.06 mM Fe(III) day^{-1}, respectively (Table S3).

With additional acetate, the Fe(II)/Fe(total) ratios in negative controls remained at 9.1 ± 4.0, 16.6 ± 8.2 and 27.4 ± 5.1% Fe(II) with freeze-thawed BIOS of TIE-1, BoFeN1 and KS, respectively. *G. sulfurreducens* reduced 100% of the freeze-thawed $BIOS_{Fe(III)}$ in 15 days (Fig. 4c). With lactate, the Fe(II)/Fe(total) ratios in negative controls remained at 9.4 ± 4.4, 16.4 ± 7.3 and 29.4 ± 8.9% with freeze-thawed BIOS of TIE-1, BoFeN1 and KS, respectively. Despite the addition of lactate, after 85 days *S. oneidensis* showed reduction extents of only 51%, 48% and 39% for BIOS of KS, BoFeN1 and TIE-1, respectively. After 267 days, an additional sampling showed that KS and BoFeN1 BIOS had been fully reduced by *S. oneidensis*, while TIE-1 BIOS only had a maximum reduction extent of 48% (Fig. 4d).

When comparing to untreated BIOS, freeze-thawing tended to decrease the $BIOS_{Fe(III)}$ reduction rates (three out of six conditions) and extents (four out of six cases) in the absence of added OC. In the presence of added OC, the reduction rates tended to be lower (five out of six conditions) while the extents tended to be comparable due to the reaction reaching completion (five out of six conditions) (Tables S2, S3). The overall decrease in reduction rates ranged from 1.5- to 10-fold lower compared to untreated BIOS. The overall decrease in reduction extent typically ranged from 10% to 20% compared to untreated BIOS, with one outlier exhibiting a 52% decrease (Tables S2, S3, S4).

Discussion

Properties of BIOS compared to the literature

Fe(III) (oxyhydr)oxides are important sinks and sources of biogeochemically important nutrients. They are known carbon sinks, trapping a substantial amount of OC in terrestrial (~40%) and marine (~19%) sediments (Jia *et al.*, 2024; Lalonde *et al.*, 2012). Extensive work has been done to study the mineral composition of BIOS and their biomineralisation patterns, particularly on the phenomenon of encrustation that occurs in some nitrate-reducing Fe(II)-oxidising bacteria (Fig. 1). Despite this, information on their basic properties (*e.g.* surface areas, zeta potential, particle size distribution, TOC) is lacking. Our work adds to this incomplete body of literature and allows comparison with previous datasets.

The SSA of BIOS has been determined to range from 158 to 286 $m^2\ g^{-1}$ (Kappler *et al.*, 2005; Piepenbrock *et al.*, 2014). We measured SSA with a range of 75–144 $m^2\ g^{-1}$ for three types of BIOS, with a value of 80 $m^2\ g^{-1}$ specifically for BoFeN1. While the SSA values are generally high and reflect their poorly crystalline nature (Song *et al.*, 2022), it seems that differences in growth conditions or culture batch could yield variation in SSA of BIOS from the same species (Table 2).

TIE-1 displayed the highest TOC (2.2 wt%), followed by BoFeN1 (1.3%) and KS (0.24%). TIE-1 is a photoferrotroph, which are known to secrete EPS to prevent encrustation (Wu *et al.*, 2014).

https://doi.org/10.1180/gbi.2026.10008 Published online by Cambridge University Press

In BoFeN1, cells are typically encrusted with Fe(III) oxyhydroxides, resulting in tight OC association within BIOS (Kappler *et al.*, 2005; Schmid *et al.*, 2014). Finally, culture KS is an autotrophic nitrate-reducing Fe(II)-oxidising co-culture, in which any OC needs to be sourced from energetically expensive fixation of CO_2. Hence, patterns in the TOC content are broadly consistent with their metabolisms. In comparison to the literature, the Fe–C content within the extracellular filaments of the photoferrotroph *Rhodobacter* sp. strain SW2 was determined to follow the relationship [Fe] = 2.5 [C] + 100 (Miot *et al.*, 2009a), while ~1.2% TOC was determined in *Gallionella*-like BIOS from groundwater (Cismasu *et al.*, 2016) (Table 2).

In this study, we measured the particle-size distribution of BIOS in suspension using a Mastersizer and a Zetasizer, revealing a broad distribution from hundreds of nanometres to a few hundred micrometers (up to ~2000 µm for TIE-1). Previous studies have used electron microscopy to estimate the size of cell-mineral aggregates in FeOB, showing that individual particles are typically <1000 nm (Huang *et al.*, 2023; Jiao *et al.*, 2005). Hence, the large size ranges we measured signify the formation of aggregates composed of minerals, cells and/or EPS in suspension. Here, the mean aggregate size for the three investigated cultures was TIE-1 > BoFeN1 > KS. The larger aggregates in TIE-1 could be induced by EPS that act as binding agents, produced by the cells to prevent cell encrustation by minerals (Wu *et al.*, 2014). In comparison, other photoferrotrophs (*Thiodictyon* sp. F4 and *Rhodobacter ferrooxidans* sp. strain SW2) also produced relatively large BIOS with a size range of 10–40 µm (as measured on a Mastersizer; Posth *et al.*, 2010) that were larger than those of BoFeN1 (mean = 11–14 µm) and KS (mean = 8 µm).

The particle-size analysis performed here also showed conclusively the presence of colloids <1200 nm in suspension, although their amount was <5% of the total Fe. These colloids have a size range of 550–1100 nm, dependent on the BIOS source and the exact culture bottle. The zeta potential for these colloids was predominantly negative, ranging from –1.0 to –5.3 mV, with one positive value for KS at +5.4 mV. These values reflect the influence of negatively charged OC on the surfaces of BIOS from deprotonated functional groups like carboxyl and phosphate groups (Ciempiel *et al.*, 2025; Huang *et al.*, 2022), as at pH 7 the zeta potential of Fe(III) (oxyhydr)oxides should be close to 0 or positive, given their point of zero charges of 7–9 (Venema *et al.*, 1996; Mansor *et al.*, 2025; Kosmulski, 2009). Overall, colloids from BIOS are present at low concentrations and tend to be negatively charged.

Disentangling factors controlling the $BIOS_{Fe(III)}$ reduction rate and extent

Following characterisation, we tested the bioavailability of BIOS for microbial Fe(III) reduction across multiple variables relevant to natural environments, resulting in a total of 24 conditions (Table S4). We therefore performed a redundancy analysis to identify the most important parameters controlling the extent and rate of $BIOS_{Fe(III)}$ reduction (Fig. 5). The analysis showed that OC addition was the main factor influencing the extent of reduction. In comparison, the rate was primarily controlled by the FeRB species, with *G. sulfurreducens* being faster than *S. oneidensis* both with and without OC. Among the BIOS sources, BoFeN1 showed the highest reduction rates, both with and without OC. Finally, freeze-thawing tended to decrease the reduction rates without affecting the extent of reduction. Below, we discuss the potential mechanisms based on these trends in more detail.

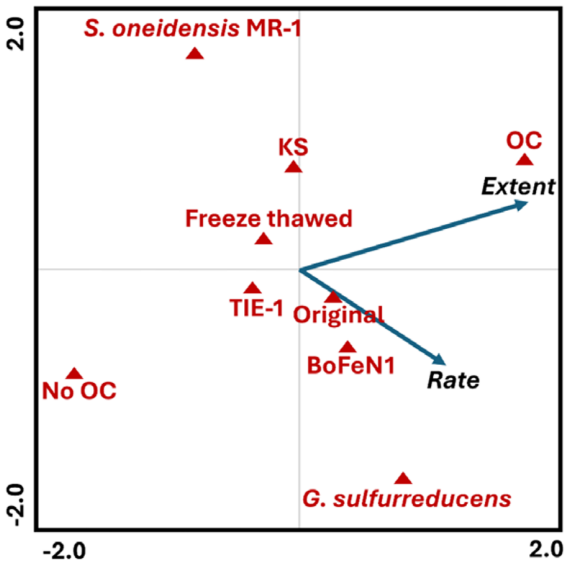


Figure 5. Redundancy analysis to determine the factors affecting the rate and extent of microbial biogenic iron oxides (BIOS) reduction. The factors evaluated were the origin of the BIOS (*Rhodopseudomonas palustris* TIE-1 (TIE-1), *Acidovorax* sp. BoFeN1 (BoFeN1), enrichment culture KS (KS)), the Fe(III)-reducing bacteria species (*G. sulfurreducens*, *S. oneidensis*), usage of additional carbon (organic carbon (OC), no OC) and BIOS treatment (original, freeze-thawed). Blue arrows are the response variables (rate and extent) and red triangles are the predictor variables. A list with the complete set of samples can be found in Table S4 and Fig. S5 displays the results including the individual samples.

Comparison of the bioavailability of BIOS with different origins and synthetic ferrihydrite

Overall, the source of the original BIOS contributed to small differences in Fe(III) reduction rates and <10% differences in reduction extent. $BIOS_{Fe(III)}$ from BoFeN1 were the most bioavailable, followed by TIE-1 and KS. The reason(s) for these differences are unclear, as they seem to be uncorrelated with their mineralogy, particle size, TOC, SSA and zeta potential (Table 2).

Compared to synthetic ferrihydrite (used due to its greater reactivity compared with other Fe(III) (oxyhydr)oxides; Han *et al.*, 2018; Glasauer *et al.*, 2003; Lovley and Phillips, 1986), the Fe(III) in all BIOS used here was more reactive and had higher reduction rates (8–13 and 1.5–5 times with *G. sulfurreducens* and *S. oneidensis*, respectively; Table S3). We attribute this greater availability to the presence of OC within BIOS. The generally negative zeta potential of the BIOS suggests the presence of organic molecules on the mineral surfaces. These organics may contain redox-active species that facilitate electron transfer between the cells and the minerals. Moreover, the presence of OC could shift the redox potential towards greater reducibility. Similar interpretations have been made in the past in relation to Fe–OC coprecipitates that showed higher reduction rates and extents compared to synthetic Fe(III) (oxyhydr)oxides (Mikutta, 2011; Poggenburg *et al.*, 2016).

We also considered two additional factors: mineralogy and surface areas. Mineralogy-wise, because BIOS contained goethite, we would expect it should have a lower bioavailability compared to synthetic ferrihydrite. Similarly, as ferrihydrite typically has a very large surface area (>200–400 $m^2\ g^{-1}$; He *et al.*, 2025; Macera *et al.*, 2020; Brinza, 2022), we would expect BIOS to be less bioavailable compared to ferrihydrite. Hence, it seems that despite these factors, the presence of redox-active species covering the minerals in BIOS

https://doi.org/10.1180/gbi.2026.10008 Published online by Cambridge University Press

results in a stronger effect with higher reduction rates. This concurs with the previously demonstrated greater bioavailability of $BIOS_{Fe(III)}$ from environmental samples compared to ferrihydrite, with BIOS being reduced 1.5–3 times more quickly than ferrihydrite (Langley *et al.*, 2009a). Our results conclusively show the high bioavailability of BIOS for microbial Fe(III) reduction. They further highlight the importance of using environmentally relevant materials such as BIOS instead of purely synthetic minerals to derive reduction rates and extents relevant to nature.

Bioavailable OC controls the extent of $BIOS_{Fe(III)}$ reduction

In setups where *G. sulfurreducens* and *S. oneidensis* were incubated with only BIOS, $BIOS_{Fe(III)}$ reduction was incomplete, with a maximum extent of 52% (of ~6 mM Fe(III)) across all BIOS. The $BIOS_{Fe(III)}$ reduction in these setups is attributed to the small yet present OC transferred from the precultures. In the case of *G. sulfurreducens*, because of the absence of washing, ~0.17 mM of acetate could be transferred from the preculture, enough to reduce ~1.36 mM of Fe, which is consistent with the ~2.0 mM of Fe(II) produced (Eq. 2) (considering this includes ~0.61 mM of initial Fe(II)). Likewise, *S. oneidensis* may contain ~1 mM of lactate coming from the preculture, enough to reduce 4 mM of Fe, which is higher than the ~1.9 mM of Fe(II) produced (Eq. 3).

$$CH_3COO^- + 8Fe(OH)_3 + 17H^+ \rightarrow 2CO_2 + 8Fe^{2+} + 22H_2O \quad (2)$$

$$C_3H_5O_3^- + 4Fe(OH)_3 + 8H^+ \rightarrow CH_3COO^- + CO_2 + 4Fe^{2+} + 11H_2O \quad (3)$$

When incubation was performed in the presence of excess of electron donor by adding acetate/lactate, all the $BIOS_{Fe(III)}$ was reduced (Fig. 3), which confirms the high bioavailability of $BIOS_{Fe(III)}$. This result also highlights the limited bioavailability of BIOS-associated organic carbon ($BIOS_{OC}$) to *G. sulfurreducens* and *S. oneidensis.* $BIOS_{OC}$ could have been inaccessible because of the complexity of the organic molecules, strong chemical bonding between Fe and C, or physical inhibition by the Fe(III) oxyhydroxides. In fact, neither of the FeRB is known to degrade high-molecular-weight molecules, apart from reducing disulfide bonds in organic matter (Phan *et al.*, 2024; Voordeckers *et al.*, 2010). In the presence of EPS – a main component of $BIOS_{OC}$ – Fe(III) oxyhydroxides displayed lower reduction rates than with natural organic matter (Cooper *et al.*, 2017; Gao *et al.*, 2019; Poggenburg *et al.*, 2018). Furthermore, as a result of aggregation, OC could be trapped within aggregate pores, making it less accessible to degradation. These combined factors contribute to limited bioavailability of $BIOS_{OC}$ to the two model FeRB species we tested here. The bioavailability of $BIOS_{OC}$ to other FeRB and microbial species (*e.g.* fermenters) remains an open question.

FeRB-specific differences in $BIOS_{Fe(III)}$ reduction

Intriguingly, *G. sulfurreducens* generally displayed higher $BIOS_{Fe(III)}$ reduction rates compared to *S. oneidensis.* We considered two factors to account for this difference. First, as the initial cell numbers were the same (~10^5 cells mL^{-1}), differences in the Fe(III) reduction rate cannot be explained by this parameter and suggest that *G. sulfurreducens* has a faster cell-specific reduction rate. However, we did not track differences in cell numbers as the incubation proceeded. Second, we considered differences in reduction mechanisms between the two FeRB. *G. sulfurreducens* preferentially reduces Fe(III) via direct cell-mineral contact, aided by electron transfer via conductive pili (Ueki, 2021). In contrast, *S. oneidensis* preferentially uses electron shuttles (*e.g.* quinone moieties), which are known to enhance the reduction of Fe(III) and allow longer electron transfer distances to the terminal electron acceptor (Chen *et al.*, 2017; Lovley and Blunt-Harris, 1999; Meng *et al.*, 2018). In the absence of added electron shuttles, *S. oneidensis* typically needs time in the order of 48–50 h to synthesise their own electron shuttles (*e.g.* flavins) (Marsili *et al.*, 2008; Von Canstein *et al.*, 2008) or to adapt to a direct contact mechanism (Kotloski and Gralnick, 2013; Lies *et al.*, 2005), which may explain their longer lag phase compared to *G. sulfurreducens* in our setups.

Previous experiments have shown differing Fe(III) reduction rates of Fe–OC coprecipitates by *Shewanella* and *Geobacter* species, depending on the C/Fe ratio. Increasing C/Fe ratios led to faster Fe(III) reduction for *Shewanella*, attributed to the presence of quinone-containing molecules acting as electron shuttles. In contrast, increasing C/Fe ratios led to slower Fe(III) reduction for *Geobacter*, attributed to a surface passivation effect that prevents *Geobacter* from attacking mineral surfaces (Cooper *et al.*, 2017). Thus, organic matter can influence the Fe(III) reduction rate of different FeRB species. In comparison to our experiment, two observations are important. First, the molar C/Fe ratios of 0.02, 0.10 and 0.17 for BIOS of KS, BoFeN1 and TIE-1, respectively, are at the low end of those observed for Fe–OC coprecipitates. Even at these low C/Fe ratios, a significant enhancement of reduction was observed for both *Geobacter* and *Shewanella* compared to ferrihydrite, attributed to the presence of redox-active species that enhanced electron transfer between cells and minerals (Martinez and Alvarez, 2018; Poggenburg *et al.*, 2016). Second, at comparable C/Fe ratios, the Fe(III) reduction rates for *Geobacter* were always faster than for *S. oneidensis* (Cooper *et al.*, 2017; Eusterhues *et al.*, 2014a, 2014b; Lovley, 1991). Our results are therefore consistent with previous studies and further highlight the higher Fe(III) reduction rates of *Geobacter* compared to *Shewanella* species.

Effect of freeze-thawing on the properties of BIOS

Freeze-thawing is a process relevant to high-latitude zones, mountain glaciers and other temperate climate regions across Earth (Hayashi, 2013). As Fe-cycling bacteria are active in these environments, it is imperative to understand the effects of freeze-thawing on the properties and bioavailability of BIOS (Nixon *et al.*, 2017; Laufer-Meiser *et al.*, 2021; Michaud *et al.*, 2023; Toubes-Rodrigo *et al.*, 2021). We found the effect of freeze-thawing to be complex and dependent on multiple parameters. For example, freeze-thawing consistently decreased the surface charges of colloidal BIOS regardless of origin. We speculate that this is due to the breakdown of complex organic molecules (*e.g.* cells and EPS) during freezing (Fellman *et al.*, 2008; Pokrovsky *et al.*, 2018) followed by their migration to the outer surface of the BIOS aggregates on thawing (Gu *et al.*, 1995). This process did not lead to changes in the TOC of BIOS of BoFeN1, while significantly ($\alpha = 0.05, n = 3$) decreasing the TOC content of TIE-1 and KS BIOS.

Freezing probably led to changes in the BIOS structure, as inferred from changes in SSA and particle-size distribution. In the case of TIE-1, the decrease in SSA and particle size indicated freezing-induced compaction. For BoFeN1, the increases in SSA and particle size were more consistent with aggregation into an open structure with high accessibility to reactive sites. In the case of

https://doi.org/10.1180/gbi.2026.10008 Published online by Cambridge University Press

KS, the decrease in SSA coupled with an increase in particle size distribution implied aggregation to larger structures with limited access to reactive surfaces. We note, however, that these are only interpretations, as the Mastersizer and Zetasizer only measure the hydrodynamic diameter, *i.e.* it assumes a hypothetical hard sphere in solution, including its surface structure and solvation layer, without giving insight into the three-dimensional arrangement of the BIOS after freeze-thawing.

Lastly, freezing did not cause a change in mineralogy nor a large difference in crystallinity of the BIOS. Freeze-thawing also potentially caused a slight increase from a Fe(II)/Fe(total) ratio of 6.9 ± 0.6%, 13.4 ± 0.3% and 27.1 ± 0.5% to 9.3 ± 4.2%, 16.6 ± 7.8% and 28.2 ± 7.5% for BIOS of TIE-1, BoFeN1 and KS, respectively, although the values still overlap if we consider the high standard deviations.

Effect of freeze-thawing on the bioavailability of BIOS

In general, freeze-thawing tended to decrease the bioavailability of $BIOS_{Fe(III)}$, although the effect is specific to the variables tested. One potential reason is the more negative surface charge that developed on BIOS on freezing. Because microbial cell membranes are generally negative, accessing the surface of BIOS via direct contact becomes more difficult when electrostatic repulsion needs to be overcome (Chorover, 2022; Marshall *et al.*, 1971; Mills, 2003).

To gain additional insight into the effect of freeze-thawing on bioavailability, we first considered setups in which additional labile OC was added. In most cases, the reduction extents reached 100%, highlighting the high bioavailability of $BIOS_{Fe(III)}$ even after freeze-thawing. The one exception is for TIE-1 BIOS reduced by *S. oneidensis*, in which case the reaction stopped at 48% reduction extent – we consider this to be an outlier. In five out of six conditions, the reduction rates were lower after freeze-thawing. This emphasises the lower accessibility of BIOS on freeze-thawing. The one exception was for BoFeN1 BIOS reduced by *G. sulfurreducens*, which exhibited a higher rate after freeze-thawing. This is perhaps related to the difference in the reduction mechanism of the respective FeRB and their response to the spatial Fe–OC association within BIOS on freeze-thawing.

Next, we consider cases in which no labile OC was added. Here, TIE-1 BIOS displayed lower reduction rates and extents with both FeRB. This is consistent with the expectation of lower bioavailability due to decreased SSA and particle size after freeze-thawing. In comparison, BoFeN1 BIOS displayed lower or comparable reduction rates after freeze-thawing. This is not expected based on its increase in SSA, but is consistent with its increase in particle size that may have led to lower accessibility to the FeRB after freeze-thawing. In contrast to the other two BIOS, KS BIOS displayed higher reduction rate and extent after freeze-thawing. This is surprising considering the decrease in SSA and increase in particle size after freeze-thawing. Overall, our results suggest that SSA and particle size are poor predictors of relative reduction rate and extent after freeze-thawing treatment. This highlights the necessity of performing microbial reduction experiments to directly measure bioavailability in the presence of multiple completing variables.

Conclusion

As the transformation of Fe minerals interlinks with other elemental cycles (*e.g.* C, N and P), here we investigated the bioavailability of BIOS from FeOB. We tested multiple variables relevant across different environments: three different origins of BIOS, two model FeRB, with and without OC, and before and after freeze-thawing. Based on RDA, our study shows that OC availability is the primary factor controlling the bioavailability of $BIOS_{Fe(III)}$. In the presence of excess labile OC, $BIOS_{Fe(III)}$ can be completely reduced, exhibiting higher reduction rates compared to synthetic ferrihydrite. This is even more surprising considering that BIOS are composed of mixtures of ferrihydrite with more crystalline lepidocrocite and goethite. Hence, it emphasises the need to conduct experiments with naturally relevant materials to avoid underestimation of reaction rates relevant to the environment.

In soils that undergo freeze-thawing, such as high-altitude zones or mountain glaciers, Fe–organic matter associations and the physical properties of the minerals are potentially altered, leading to different bioavailability of the minerals and OC. The impact of freeze-thawing in BIOS properties (particle-size distribution, SSA and TOC) was FeOB-specific. Only the effect on their zeta potential was consistent, increasing their magnitude towards more negative values in all BIOS. These changes in the properties had a greater impact on the rate than on the extent of reduction. Overall, freeze-thawing was a secondary control on bioavailability, with the primary factor being the presence of labile OC.

Our study also indicated limited bioavailability of the $BIOS_{OC}$ for FeRB, although we cannot exclude its bioavailability in natural systems, where other microorganisms (*e.g.* fermentative microorganisms) could degrade and transform the associated OC to more bioavailable low-molecular-weight organic molecules. We leave this open question for further studies. We attempted to directly track if any $BIOS_{OC}$ was released to the solution. However, the low TOC content of BIOS (0.24–2.2 wt%) made this challenging. Conversion to OC/Fe molar ratios revealed a range of 0.02–0.17, which is much lower than observed for natural Fe–OC aggregates, ranging from <1.0 for sorption to a maximum of 6–10 for coprecipitation or chelation (Lalonde *et al.*, 2012). Then, the role of BIOS on the fate of carbon is limited and linked to the carbon that could potentially adsorb and co-precipitate within BIOS, rather than to the amount of native $BIOS_{OC}$. We stress, however, that we worked exclusively with anaerobic FeOB in this study. Environmental BIOS collected under microoxic conditions have been found to contain up to 34.5 wt% organic matter (Martinez *et al.*, 2003). Furthermore, the higher reactivity of BIOS compared to ferrihydrite indicates that OC associated with BIOS is more likely to be released. To unequivocally trace which molecules are derived from BIOS and determine their use, other more sensitive approaches need to be undertaken in future studies, such as ^{13}C labelling during BIOS formation by Fe(II)-oxidising bacteria.

Supplementary material. The supplementary material for this article can be found at http://doi.org/10.1180/gbi.2026.10008.

Acknowledgements. The authors acknowledge support by the Deutsche Forschungsgemeinschaft (DFG, German Research Foundation), Project 494840258. A.K. acknowledges infrastructural support by the DFG under Germany's Excellence Strategy, Cluster of Excellence EXC2124, project ID 390838134. The authors would like to thank Jeremiah Shuster for his assistance in the acquisition of SEM micrographs via the Tübingen Structural Microscopy Core Facility (funded by the Federal Ministry of Education and Research (BMBF) and the Baden-Württemberg Ministry of Science as part of the Excellence Strategy of the German Federal and State Governments). We also thank the German Research Foundation DFG (INST 37/1027-1 FUGG) for financial support provided for the acquisition of the cryogenic focused ion beam scanning electron microscope. Additionally, we thank Nora Kainz for her assistance in DOC measurements; Marie Mollenkopf for HPLC measurements, and Bernice

Nisch for TOC measurements. We acknowledge support from the Open Access Publishing Fund of the University of Tübingen.

References

Abramov S.M., Straub D., Tejada J., Grimm L., Schädler F., Bulaev A., Thorwarth H., Amils R., Kappler A. and Kleindienst S. (2022) Biogeochemical niches of Fe-cycling communities influencing heavy metal transport along the Rio Tinto, Spain. *Applied and Environmental Microbiology*, **88**, e02290–21.

Adhikari D., Zhao Q., Das K., Mejia J., Huang R., Wang X., Poulson S.R., Tang Y., Roden E.E. and Yang Y. (2017) Dynamics of ferrihydrite-bound organic carbon during microbial Fe reduction. *Geochimica et Cosmochimica Acta*, **212**, 221–233.

Adhikari D., Dunham-Cheatham S.M., Wordofa D.N., Verburg P., Poulson S.R. and Yang Y. (2019) Aerobic respiration of mineral-bound organic carbon in a soil. *Science of the Total Environment*, **651**, 1253–1260.

Angelova R., Groudeva V., Slavov L., Iliev M., Nedkov I., Sziklai-László I. and Krezhov K. (2015) Investigation of iron-containing products from natural and laboratory cultivated *Sphaerotilus–Leptothrix* bacteria. *Journal of Biological Physics*, **41**, 367–375.

Baker I.R., Matzen S.L., Schuler C.J., Toner B.M. and Girguis P.R. (2023) Aerobic iron-oxidizing bacteria secrete metabolites that markedly impede abiotic iron oxidation. *PNAS Nexus*, **2**, pgad421.

Brinza L., (2022) Surface coverage simulation and 3D plotting of main process parameters for molybdenum and vanadium adsorption onto ferrihydrite. *Nanomaterials*, **12**, 304.

Brooks C.N. and Field E.K. (2020) Iron flocs and the three domains: microbial interactions in freshwater iron mats. *mBio*, **11**, e02720–20.

Brunauer S., Emmett P.H. and Teller E. (1938) Adsorption of gases in multimolecular layers. *Journal of the American Chemical Society*, **60**, 309–319.

Chan C.S., Fakra S.C., Edwards D.C., Emerson D. and Banfield J.F. (2009) Iron oxyhydroxide mineralization on microbial extracellular polysaccharides. *Geochimica et Cosmochimica Acta*, **73**, 3807–3818.

Chen Z., Wang Y., Jiang X., Fu D., Xia D., Wang H., Dong G. and Li Q. (2017) Dual roles of AQDS as electron shuttles for microbes and dissolved organic matter involved in arsenic and iron mobilization in arsenic-rich sediment. *Science of the Total Environment*, **574**, 1684–1694.

Chen S.C., Li X.M., Battisti N., Guan G., Montoya M.A., Osvatic J., Pjevac P., Pollak S., Richter A., Schintlmeister A., Wanek W., Mussmann M. and Loy A. (2025) Microbial iron oxide respiration coupled to sulfide oxidation. *Nature*, **646**(8086), 925–933. https://doi.org/10.1038/s41586-025-09467-0.

Chorover, J. (2022). Microbe–biomolecule–mineral interfacial reactions. Multi-Scale Biogeochemical Processes in Soil Ecosystems: Critical Reactions and Resilience to Climate Changes, 117–140. https://doi.org/10.1002/9781119480419.ch5

Ciempiel W., Czemierska M., Wiącek D., Szymańska M., Jarosz-Wilkołazka A., Krzemińska I. (2025) Lead biosorption and chemical composition of extracellular polymeric substances isolated from mixotrophic microalgal cultures. *Scientific Reports*, **15**, 9093.

Cismasu A.C., Williams K.H. and Nico P.S. (2016) Iron and carbon dynamics during aging and reductive transformation of biogenic ferrihydrite. *Environmental Science & Technology*, **50**, 25–35.

Cooper R.E., Eusterhues K., Wegner C.-E., Totsche K.U. and Küsel K. (2017) Ferrihydrite-associated organic matter stimulates reduction by *Shewanella oneidensis* MR-1 and a complex microbial consortia. *Biogeosciences*, **14**, 5171–5188.

Deville S. (2017) Freezing colloids: observations, principles, control and use. Pp. xx–xx in: *Applications in Materials Science, Life Science, Earth Science, Food Science and Engineering*. Springer International Publishing.

Druschel G.K., Emerson D., Sutka R., Suchecki P. and Luther G.W. (2008) Low-oxygen and chemical kinetic constraints on the geochemical niche of neutrophilic iron(II) oxidizing microorganisms. *Geochimica et Cosmochimica Acta*, **72**(14), 3358–3370. https://doi.org/10.1016/j.gca.2008.04.035.

Ehrenreich A. and Widdel F. (1994) Anaerobic oxidation of ferrous iron by purple bacteria, a new type of phototrophic metabolism. *Applied and Environmental Microbiology*, **60**(12), 4517–4526. https://doi.org/10.1128/aem.60.12.4517-4526.1994.

Eusterhues, K., Hädrich, A., Neidhardt, J., Küsel, K., Keller, T. F., Jandt, K. D. and Totsche, K. U. (2014a) Reduction of ferrihydrite with adsorbed and coprecipitated organic matter: Microbial reduction by *Geobacter bremensis* vs. abiotic reduction by Na-dithionite. *Biogeosciences*, **11**, 4953–4966.

Eusterhues, K., Neidhardt, J., Hädrich, A., Küsel, K. and Totsche, K. U. (2014b) Biodegradation of ferrihydrite-associated organic matter. *Biogeochemistry*, **119**, 45–50.

Fellman J.B., D'Amore D.V. and Hood E. (2008) An evaluation of freezing as a preservation technique for analyzing dissolved organic C, N and P in surface water samples. *Science of the Total Environment*, **392**, 305–312.

Ferris F.G. (2005) Biogeochemical properties of bacteriogenic iron oxides. *Geomicrobiology Journal*, **22**, 79–85.

Gao L., Lu X., Liu H. Li J., Li W., Song R., Wang R., Zhang D. and Zhu, J. (2019) Mediation of extracellular polymeric substances in microbial reduction of hematite by *Shewanella oneidensis* MR-1. *Frontiers in Microbiology*, **10**, 575. https://doi.org/10.3389/fmicb.2019.00575.

Garber A.I., Cohen A.B., Nealson K.H., Ramírez G.A., Barco R.A., Enzingmüller-Bleyl T.C., Gehringer M.M. and Merino N. (2021) Metagenomic insights into the microbial iron cycle of subseafloor habitats. *Frontiers in Microbiology*, **12**, 1–18.

Gault A.G., Langley S., Ibrahim A. Renaud R., Takahashi Y., Boothman C., Lloyd J.R., Clark I.D., Ferris F.G. and Fortin, D. (2012) Seasonal changes in mineralogy, geochemistry and microbial community of bacteriogenic iron oxides (BIOs) deposited in a circumneutral wetland. *Geomicrobiology Journal*, **29**(2), 161–172. https://doi.org/10.1080/01490451.2010.532196

Glasauer, S., Weidler, P.G., Langley, S. and Beveridge, T.J. (2003) Controls on Fe reduction and mineral formation by a subsurface bacterium. *Geochimica et Cosmochimica Acta*, **67**, 1277–1288. https://doi.org/10.1016/S0016-7037(02)01199-7

Goebel M.-O., Bachmann J., Woche S.K. and Fischer W.R. (2005) Soil wettability, aggregate stability, and the decomposition of soil organic matter. *Geoderma*, **128**, 80–93.

Gu B., Schmitt J., Chen Z., Liang L. and McCarthy J.F. (1995) Adsorption and desorption of different organic matter fractions on iron oxide. *Geochimica et Cosmochimica Acta*, **59**, 219–229.

Han R., Liu T., Li F., Li X., Chen D. and Wu Y. (2018) Dependence of secondary mineral formation on Fe(II) production from ferrihydrite reduction by *Shewanella oneidensis* MR-1. *ACS Earth and Space Chemistry*, **2**, 399–409.

Hayashi M. (2013) The cold vadose zone: hydrological and ecological significance of frozen-soil processes. *Vadose Zone Journal*, **12**, 1–8.

He B., Zhang W., Diao Y., Sun S., Zhang Y., Zhao W., Wen F. and Yang G. (2025) Mechanistic study of the adsorption capabilities of heavy metals on the surface of ferrihydrite: batch sorption, modeling, and density functional theory. *RSC Advances*, **15**(2), 1072–1080. https://doi.org/10.1039/D4RA07426B.

Hegler F., Posth N.R., Jiang J. and Kappler A. (2008) Physiology of phototrophic iron(II)-oxidizing bacteria: implications for modern and ancient environments. *FEMS Microbiology Ecology*, **66**, 250–260.

Huang L., Jin Y., Zhou D. Liu L., Huang S., Zhao Y. and Chen Y. (2022) A review of the role of extracellular polymeric substances (EPS) in wastewater treatment systems. *International Journal of Environmental Research and Public Health*, **19**(19), 12191. https://doi.org/10.3390/ijerph191912191.

Huang J., Mellage A., Garcia J.P., Glöckler D., Mahler S., Elsner M., Jakus N., Mansor M., Jiang H. and Kappler A. (2023) Metabolic performance and fate of electrons during nitrate-reducing Fe(II) oxidation by the autotrophic enrichment culture KS grown at different initial Fe/N ratios. *Applied and Environmental Microbiology*, **89**, e00196–23.

Hunter R.J. (1981) *Zeta Potential in Colloid Science: Principles and Applications*. Academic Press.

Jeong, D., Kim, K., Min, D. W., & Choi, W. (2015). Freezing-enhanced dissolution of iron oxides: effects of inorganic acid anions. *Environmental Science & Technology*, **49**(21), 12816–12822. https://doi.org/10.1021/acs.est.5b04211.

Jia N., Li L., Guo H. and Xie M. (2024) Important role of Fe oxides in global soil carbon stabilization and stocks. *Nature Communications*, **15**, 10318.

Jiao Y., Kappler A., Croal L.R. and Newman D.K. (2005) Isolation and characterization of a genetically tractable photoautotrophic Fe(II)-oxidizing bacterium, *Rhodopseudomonas palustris* strain TIE-1. *Applied and Environmental Microbiology*, **71**, 4487–4496.

Kappler A., Schink B. and Newman D.K. (2005) Fe(III) mineral formation and cell encrustation by the nitrate-dependent Fe(II)-oxidizer strain BoFeN1. *Geobiology*, **3**, 235–245.

Kappler A., Bryce C., Mansor M., Lueder U., Byrne J.M. and Swanner E.D. (2021) An evolving view on biogeochemical cycling of iron. *Nature Reviews Microbiology*, **19**(6), 360–374. https://doi.org/10.1038/s41579-020-00502-7.

Kikuchi S., Makita H., Takai K., Yamaguchi N. and Takahashi Y. (2014) Characterization of biogenic iron oxides collected by the newly designed liquid culture method using diffusion chambers. *Geobiology*, **12**, 133–145.

Knoll A.H., Canfield D.E. and Konhauser K.O. (2012) *Fundamentals of Geobiology*. 1st ed. John Wiley & Sons, Incorporated.

Konhauser K.O., Kappler A. and Roden E.E. (2011) Iron in microbial metabolisms. *Elements*, **7**(2), 89–93. https://doi.org/10.2113/gselements.7.2.89.

Kosmulski M. (2009) Compilation of PZC and IEP of sparingly soluble metal oxides and hydroxides from literature. *Advances in Colloid and Interface Science*, **152**, 14–25.

Kotloski N.J. and Gralnick J.A. (2013) Flavin electron shuttles dominate extracellular electron transfer by *Shewanella oneidensis* MR-1. *mBio*, **4**, e00553–12.

Kubannek F., Thiel S., Bunk B., Huber K., Overmann J., Krewer U., Biedendieck R. and Jahn D. (2020) Performance modelling of the bioelectrochemical glycerol oxidation by a co-culture of *Geobacter sulfurreducens* and *Raoultella electrica*. *ChemElectroChem*, **7**, 1877–1888.

Lagarec K. and Rancourt D.G. (1997) Extended Voigt-based analytic lineshape method for determining N-dimensional correlated hyperfine parameter distributions in Mössbauer spectroscopy. *Nuclear Instruments and Methods in Physics Research Section B: Beam Interactions with Materials and Atoms*, **129**(2), 266–280.

Lalonde K., Mucci A., Ouellet A. and Gélinas Y. (2012) Preservation of organic matter in sediments promoted by iron. *Nature*, **483**, 198–200.

Langley S., Gault A., Ibrahim A., Renaud R., Fortin D., Clark I.D. and Ferris F.G. (2009a) A comparison of the rates of Fe(III) reduction in synthetic and bacteriogenic iron oxides by *Shewanella putrefaciens* CN32. *Geomicrobiology Journal*, **26**, 57–70.

Langley S., Igric P., Takahashi Y., Sakai Y., Fortin D., Hannington M.D. and Schwarz-Schampera U. (2009b) Preliminary characterization and biological reduction of putative biogenic iron oxides (BIOS) from the Tonga-Kermadec Arc, southwest Pacific Ocean. *Geobiology*, **7**(1), 35–49. https://doi.org/10.1111/j.1472-4669.2008.00180.x.

Laufer-Meiser K., Michaud A.B., Maisch M., Byrne J.M., Kappler A., Patterson M.O., Røy H. and Jørgensen B.B. (2021) Potentially bioavailable iron produced through benthic cycling in glaciated Arctic fjords of Svalbard. *Nature Communications*, **12**(1), 1349. https://doi.org/10.1038/s41467-021-21558-w.

Lies D.P., Hernandez M.E., Kappler A., Mielke R.E., Gralnick J.A. and Newman D.K. (2005) *Shewanella oneidensis* MR-1 uses overlapping pathways for iron reduction at a distance and by direct contact under conditions relevant for biofilms. *Applied and Environmental Microbiology*, **71**, 4414–4426.

Lovley, D.R. and Phillips, E.J.P. (1986) Availability of ferric iron for microbial reduction in bottom sediments of the freshwater tidal Potomac River. *Applied and Environmental Microbiology*, **52**, 751–757. https://doi.org/10.1128/aem.52.4.751-757.1986.

Lovley D.R. (1991) Dissimilatory Fe(III) and Mn(IV) reduction. *Microbiological Reviews*, **55**, 259–287.

Lovley D.R. and Blunt-Harris E.L. (1999) Role of humic-bound iron as an electron transfer agent in dissimilatory Fe(III) reduction. *Applied and Environmental Microbiology*, **65**, 4252–4254.

Macera L., Taglieri G., Daniele V., Passacantando M. and D'Orazio F. (2020) Nano-sized Fe(III) oxide particles starting from an innovative and eco-friendly synthesis method. *Nanomaterials*, **10**, 323.

Mansor M., Duverger A., Pasquier V., Gorlas A., Guyot F., Berg J.S., Marine-Carbonne J., Cosmidis J. and Picard A. (2025) Biogenic pyrite and metastable iron sulfides: emerging formation pathways and geological and societal relevance. *Geo-bio Interfaces*, **2**, e6.

Marshall, K.C., Stout, R., and Mitchell, R. (1971). Mechanism of initial events in sorption of marine bacteria to surfaces. *Journal of General Microbiology*, **68**: 337–348. https://doi.org/10.1099/00221287-68-3-337.

Marsili E., Baron D.B., Shikhare I.D., Coursolle D., Gralnick J.A. and Bond D.R. (2008) *Shewanella* secretes flavins that mediate extracellular electron transfer. *Proceedings of the National Academy of Sciences*, **105**, 3968–3973.

Martinez C.M. and Alvarez L.H. (2018) Application of redox mediators in bioelectrochemical systems. *Biotechnology Advances*, **36**, 1412–1423.

Martinez R.E., Smith D.S., Pedersen K. and Ferris F.G. (2003) Surface chemical heterogeneity of bacteriogenic iron oxides from a subterranean environment. *Environmental Science & Technology*, **37**, 5671–5677.

Meng Y., Zhao Z., Burgos W.D., Li Y., Zhang B., Wang Y., Liu W., Sun L., Lin L. and Luan F. (2018) Iron(III) minerals and anthraquinone-2,6-disulfonate (AQDS) synergistically enhance bioreduction of hexavalent chromium by *Shewanella oneidensis* MR-1. *Science of The Total Environment*, 640–641, 591–598.

Michaud A.B., Massé R.O. and Emerson D. (2023) Microbial iron cycling is prevalent in water-logged Alaskan Arctic tundra habitats, but sensitive to disturbance. *FEMS Microbiology Ecology*, **99**, fiad013.

Mikutta C. (2011) X-ray absorption spectroscopy study on the effect of hydroxybenzoic acids on the formation and structure of ferrihydrite. *Geochimica et Cosmochimica Acta*, **75**, 5122–5139.

Mills, A. L. (2003). Keeping in touch: microbial life on soil particle surfaces. *Advances in Agronomy*, **78**, 2–45. https://doi.org/10.1016/s0065-2113(02)78001.

Miot J., Benzerara K., Obst M., Kappler A., Hegler F., Schädler S., Bouchez C., Guyot F. and Morin G. (2009a) Extracellular iron biomineralization by photoautotrophic iron-oxidizing bacteria. *Applied and Environmental Microbiology*, **75**, 5586–5591.

Miot J., Benzerara K., Morin G., Kappler A., Bernard S., Obst M., Férard C., Skouri-Panet F., Guigner J.-M., Posth N. *et al.* (2009b) Iron biomineralization by anaerobic neutrophilic iron-oxidizing bacteria. *Geochimica et Cosmochimica Acta*, **73**, 696–711.

Miot J., Remusat L., Duprat E., Gonzalez A., Pont S. and Poinsot M. (2015) Fe biomineralization mirrors individual metabolic activity in a nitrate-dependent Fe(II)-oxidizer. *Frontiers in Microbiology*, **6**, 879.

Mullin J.W. (2004) *Crystallization*. 4th ed. Butterworth-Heinemann.

Najem T., Langley S. and Fortin D. (2016) A comparison of Fe(III) reduction rates between fresh and aged biogenic iron oxides (BIOS) by *Shewanella putrefaciens* CN32. *Chemical Geology*, **439**, 1–12.

Nedkov I., Slavov L., Angelova R., Blagoev B., Kovacheva D., Abrashev M.V., Iliev M. and Groudeva V. (2016) Biogenic nanosized iron oxides obtained from cultivation of iron bacteria from the genus *Leptothrix*. *Journal of Biological Physics*, **42**, 587–600.

Nikeleit V., Maisch M., Byrne J.M., Harwood C., Kappler A. and Bryce C. (2024) Phototrophic Fe(II) oxidation by *Rhodopseudomonas palustris* TIE-1 in organic and Fe(II)-rich conditions. *Environmental Microbiology*, **26**, e16608.

Nixon S.L., Telling J.P., Wadham J.L. and Cockell C.S. (2017) Viable cold-tolerant iron-reducing microorganisms in geographically diverse subglacial environments. *Biogeosciences*, **14**, 1445–1455.

Patterson A.L. (1939) The Scherrer formula for X-ray particle size determination. *Physical Review*, **56**(10), 978–982. https://doi.org/10.1103/PhysRev.56.978.

Patzner M.S., Mueller C.W., Malusova M., Baur M., Nikeleit V., Scholten T., Hoeschen C., Byrne J.M., Borch T., Kappler A. and Bryce C. (2020) Iron mineral dissolution releases iron and associated organic carbon during permafrost thaw. *Nature Communications*, **11**(1), 6329. https://doi.org/10.1038/s41467-020-20102-6.

Patzner M.S., Kainz N., Lundin E., Barczok M., Smith C., Herndon E., Kinsman-Costello L., Fischer S., Straub D., Kleindienst S., Kappler A. and Bryce C. (2022) Seasonal fluctuations in iron cycling in thawing permafrost peatlands. *Environmental Science & Technology*, **56**(7), 4620–4631. https://doi.org/10.1021/acs.est.1c06937.

Payandi-Rolland D., Shirokova L.S., Labonne F., Bénézeth P. and Pokrovsky O.S. (2021) Impact of freeze-thaw cycles on organic carbon and metals in waters of permafrost peatlands. *Chemosphere*, **279**, 130510.

Phan J., Macwan S., Gralnick J.A. and Yee N. (2024) Extracellular organic disulfide reduction by *Shewanella oneidensis* MR-1. *Microbiology Spectrum*, **12**, e04081–23.

Piepenbrock, A., Schröder, C., & Kappler, A. (2014). Electron transfer from humic substances to biogenic and abiogenic Fe(III) oxyhydroxide minerals.

Environmental Science and Technology, **48**(3), 1656–1664. https://doi.org/10.1021/es404497h.

Poggenburg C., Mikutta R., Sander M., Schippers A., Marchanka A., Dohrmann R. and Guggenberger G. (2016) Microbial reduction of ferrihydrite-organic matter coprecipitates by *Shewanella putrefaciens* and *Geobacter metallireducens* in comparison to mediated electrochemical reduction. *Chemical Geology*, **447**, 133–147.

Poggenburg C., Mikutta R., Schippers A., Dohrmann R. and Guggenberger G. (2018) Impact of natural organic matter coatings on the microbial reduction of iron oxides. *Geochimica et Cosmochimica Acta*, **224**, 223–248.

Pokrovsky O.S., Karlsson J. and Giesler R. (2018) Freeze-thaw cycles of Arctic thaw ponds remove colloidal metals and generate low-molecular-weight organic matter. *Biogeochemistry*, **137**, 321–336.

Porras R.C., Hicks Pries C.E., Torn M.S. and Nico P.S. (2018) Synthetic iron (hydr)oxide-glucose associations in subsurface soil: effects on decomposability of mineral-associated carbon. *Science of The Total Environment*, 613–614, 342–351.

Posth N.R., Huelin S., Konhauser K.O. and Kappler A. (2010) Size, density and composition of cell–mineral aggregates formed during anoxygenic phototrophic Fe(II) oxidation: impact on modern and ancient environments. *Geochimica et Cosmochimica Acta*, **74**, 3476–3493.

Putnis A. (2009) Mineral replacement reactions. *Reviews in Mineralogy and Geochemistry*, **70**, 87–124.

Roden E.E. (2003) Fe(III) oxide reactivity toward biological versus chemical reduction. *Environmental Science & Technology*, **37**, 1319–1324.

Roden E.E. (2004) Analysis of long-term bacterial vs. chemical Fe(III) oxide reduction kinetics. *Geochimica et Cosmochimica Acta*, **68**, 3205–3216.

Schmid G., Zeitvogel F., Hao L., Ingino P., Floetenmeyer M., Stierhof Y.-D., Schroeppel B., Burkhardt C.J., Kappler A. and Obst M. (2014) 3-D analysis of bacterial cell-(iron)mineral aggregates formed during Fe(II) oxidation by the nitrate-reducing *Acidovorax* sp. strain BoFeN1 using complementary microscopy tomography approaches. *Geobiology*, **12**, 340–361.

Schwertmann U. and Cornell R.M. (2008) *Iron oxides in the laboratory: preparation and characterization*. John Wiley & Sons.

Sebaaly, A. P., van Rijn, F., Hanna, K., & Boily, J. F. (2025). Ice as a kinetic and mechanistic driver of oxalate-promoted iron oxyhydroxide dissolution. *Proceedings of the National Academy of Sciences*, **122**(35), e2507588122. https://doi.org/10.1073/pnas.2507588122.

Song X., Wang P., Van Zwieten L., Bolan N., Wang H., Li X., Cheng K., Yang Y., Wang M., Liu T. and Li, F. (2022) Towards a better understanding of the role of Fe cycling in soil for carbon stabilization and degradation. *Carbon Research*, **1**(1), 5. https://doi.org/10.1007/s44246-022-00008-2.

Sowers T.D., Holden K.L., Coward E.K. and Sparks D.L. (2019) Dissolved organic matter sorption and molecular fractionation by naturally occurring bacteriogenic iron (oxyhydr)oxides. *Environmental Science & Technology*, **53**, 4295–4304.

Stookey L.L. (1970) Ferrozine—A new spectrophotometric reagent for iron. *Analytical Chemistry*, **42**, 779–781.

Straub K.L., Hanzlik M. and Buchholz-Cleven B.E.E. (1998) The use of biologically produced ferrihydrite for the isolation of novel iron-reducing bacteria. *Systematic and Applied Microbiology*, **21**, 442–449.

Tian Y., Abulaizi M., Yang Z., Kou T., Jia Y., Hu Y., Chen M. and Jia H. (2025) Iron-oxidizing microorganisms affect the iron-bound organic carbon in the subsoil of alpine grassland during the thawing of seasonal frozen soil. *Frontiers in Microbiology*, **15**, 1523084.

Toner B.M., Santelli C.M., Marcus M.A., Wirth R., Chan C.S., McCollom T., Bach W. and Edwards K.J. (2009) Biogenic iron oxyhydroxide formation at mid-ocean ridge hydrothermal vents: Juan de Fuca Ridge. *Geochimica et Cosmochimica Acta*, **73**, 388–403.

Toubes-Rodrigo M., Potgieter-Vermaak S., Sen R., Oddsdóttir E.S., Elliott D. and Cook S. (2021) Active microbial ecosystem in glacier basal ice fuelled by iron and silicate comminution-derived hydrogen. *MicrobiologyOpen*, **10**, e1200.

Trinks H., Schröder W. and Biebricher C.K. (2005) Ice and the origin of life. *Origins of Life and Evolution of Biospheres*, **35**, 429–445.

Ueki T. (2021) Cytochromes in extracellular electron transfer in *Geobacter*. *Applied and Environmental Microbiology*, **87**, e03109–20.

Venema P., Hiemstra T. and van Riemsdijk W.H. (1996) Multisite adsorption of cadmium on goethite. *Journal of Colloid and Interface Science*, **183**, 515–527.

Von Canstein H., Ogawa J., Shimizu S. and Lloyd J.R. (2008) Secretion of flavins by *Shewanella* species and their role in extracellular electron transfer. *Applied and Environmental Microbiology*, **74**, 615–623.

Voordeckers J.W., Kim B.-C., Izallalen M. and Lovley D.R. (2010) Role of *Geobacter sulfurreducens* outer surface c-type cytochromes in reduction of soil humic acid and anthraquinone-2,6-disulfonate. *Applied and Environmental Microbiology*, **76**, 2371–2375.

Whitaker A.H., Austin R.E., Holden K.L., Jones J.L., Michel F.M., Peak D., Thompson A. and Duckworth O.W. (2021) The structure of natural biogenic iron (oxyhydr)oxides formed in circumneutral pH environments. *Geochimica et Cosmochimica Acta*, **308**, 237–255.

Wu W., Swanner E.D., Hao L., Zeitvogel F., Obst M., Pan Y. and Kappler A. (2014) Characterization of the physiology and cell-mineral interactions of the marine anoxygenic phototrophic Fe(II) oxidizer *Rhodovulum iodosum*—Implications for Precambrian Fe(II) oxidation. *FEMS Microbiology Ecology*, **88**, 503–515.

Wu S., Liu C., Li X., Xiao B. and Hu Q. (2022) Freeze-thaw controlled aggregation mechanism of humic acid-coated goethite: Implications for organic carbon preservation. *Geoderma*, **406**, 115514.

Xu X., Mansor M., Li G., Chiu T.H., Haderlein S.B., Kappler A. and Joshi P. (2025) Size-dependent reduction kinetics of iron oxides in single and mixed mineral systems. *Environmental Science & Technology*, **59**, 2519–2530.

Yudina A. and Kuzyakov Y. (2019) Saving the face of soil aggregates. *Global Change Biology*, **25**, 3574–3577.

Zhai J., Zhang Z., Melnikov A., Zhang M., Yang L. and Jin D. (2021) Experimental study on the effect of freeze-thaw cycles on the mineral particle fragmentation and aggregation with different soil types. *Minerals*, **11**, 913.

https://doi.org/10.1180/gbi.2026.10008 Published online by Cambridge University Press